ACS APPLIED MATERIALS & INTERFACES

Research Article

www.acsami.org

# Use of Plasma Polymerization to Improve Adhesion Strength in Carbon Fiber Composites Cured by Electron Beam

Frédéric Vautard,*[,†,‡] Philippe Fioux,[†] Loïc Vidal,[†] Frédéric Siffer,[†] Vincent Roucoules,[†] Jacques Schultz,[†] Michel Nardin,[†] and Brigitte Defoort[‡]

[†]Institut de Science des Matériaux de Mulhouse, Université de Haute Alsace, CNRS-UMR 7361, 15 rue Jean Starcky, 68057 Mulhouse, France

[‡]EADS Astrium, Avenue du Général Niox, 33165 Saint Médard en Jalles, France

**ABSTRACT:** Maleic anhydride plasma polymer was deposited at the surface of carbon fibers and functionalized with vinyl and thiol groups to improve its adhesion strength with an acrylate matrix cured by an electron beam. A characterization of the fiber surface properties was done before and after coating (topography, surface chemistry, and surface energy). Sharp improvements of the interfacial shear strength (+ 120%), measured by a micromechanical test derived from the pull-out test, were obtained and, to the best of our knowledge, never reported before. The values were close to the ones obtained with a thermal cure. The comparison of this approach with other types of surface treatments (oxidation, grafting of coupling agents) enabled the establishment of a general strategy for the improvement of the interfacial adhesion in carbon fiber composites cured by an electron beam and potentially the improvement of their mechanical properties. This strategy is based on a high surface density of functionalities that are generating covalent bonding during the polymerization of the matrix and on the insertion of a polymer layer strongly attached to the fiber surface and acting as a buffer between the fiber surface and the matrix to counteract the generation of stress in the interphase.

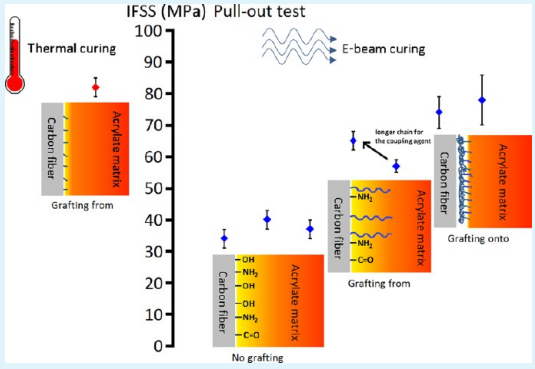


**KEYWORDS:** *carbon fiber, plasma polymerization, polymer-matrix composites (PMCs), interface, fiber/matrix bond, acrylate resin, electron beam curing*

## I. INTRODUCTION

The composite industry keeps growing, and this is particularly the case for high performance composites, as structural applications in new generation commercial airplanes were developed recently (A350 from Airbus and Dreamliner from Boeing). There is a strong demand for more energy efficient and more environmentally friendly processing, and out-of-autoclave curing technologies are gaining interest. The Electron Beam curing (EB curing) of composite materials has a lot of potential, as its energy efficiency was evaluated to be around 10 times higher than thermal treatment in an autoclave.[1] Also, fewer volatile organic compounds are generated, and the use of toxic hardeners or radical initiators is eliminated. The cure is complete within a few minutes only, and the remaining thermal stress is less important than in the case of a thermal cure.[2] Moreover, the size of the composite parts tends to increase, and it does not seem that the use of bigger autoclave devices that consume more energy is an adequate response.[3]

Nevertheless, the transverse mechanical properties, the InterLaminar Shear Strength (ILSS), and the fracture resistance[4] of composites cured by EB are typically not as good as for the best composites cured by a thermal treatment. Consequently, the overall mechanical properties of composites cured by EB cannot currently challenge the mechanical properties of the best composites cured by thermal treatment. One property that needed improvement was the toughness of the matrix, and sharp increases of the fracture resistance of resins cured by EB have been obtained.[5−7] The other property affecting the performance of EB cured composites is the adhesion strength between the fiber surface and the matrix. It was clearly demonstrated to be particularly weak with surface-treated and nonsized commercial carbon fibers,[8] so carbon fiber surface treatments and sizings adapted to EB curing have to be developed. The level of adhesion strength at the fiber/matrix interface/interphase depends on the conditions used during the manufacturing[9] and is dependent on mechanical interlocking,[10] physical[11−13] and chemical interactions,[14] the presence of defects[15] (voids, lack of cohesion), and remaining stress because of the thermal history[16] or the shrinkage of the matrix.[17] It was demonstrated that the difference of adhesion strength between EB curing and thermal curing when using nonsized commercial carbon fibers and an acrylate matrix was due to the thermal history of the sample during the cure.[18] During a thermal curing of a carbon fiber-acrylate composite, the temperature reached within the composite is high enough to create covalent bonding at the interface, which is not the

Received: October 16, 2013
Accepted: December 20, 2013
Published: December 20, 2013

  

case with the conditions that are usually used with EB curing. This is also why changing the surface properties of the carbon fiber (topography, surface chemistry) by different oxidative surface treatments (electrochemical,[19] boiling nitric acid,[20] oxygen plasma[21]) only led to very limited improvement of the adhesion strength. Of course, the irradiation conditions can be changed so that higher temperatures are generated in the composite during the cure. For example, the dose rate can be increased so that the exothermicity of the polymerization gives enough thermal energy to reach the required temperatures or the composite sample can be preheated. But the aim of the EB curing will be changed, and higher residual thermal stress will be produced. Instead, the same irradiation conditions can be used, but the carbon fiber surface has to be functionalized with chemical groups that will generate covalent bonding with the matrix during the polymerization and within the allowed processing conditions (thermal history and kinetics). If the fiber was to be sized, it would be fundamental that the composition of the sizing was compatible with the polymerization mechanism. Some epoxy-based commercial sizings had a negative influence on the interfacial mechanical properties of carbon fiber-epoxy composites cured by EB due to their composition.[22] Previous work showed that the grafting of acrylate functionalities[23] or thiol groups[24] improved the adhesion strength at the interface and the mechanical properties of the corresponding composites. Some improvement was still possible, as surface functionalities having a negative effect on the polymerization were still present at the surface of the fiber (amines, phenols). A surface treatment capable of shielding the matrix from the carbon fiber surface while supplying the compatible functional groups appeared necessary. The surface density of those functional groups, and consequently the density of covalent bonding at the interface, had to be increased also. The negative influence[25] of a high value of the cure volume shrinkage of the matrix needed to be counteracted as well.

Plasma polymerization is a technique that can potentially respond to all requirements simultaneously, as it can coat the fiber with a polymer film of controlled structure and mechanical properties and with a high surface density of specific functional groups, depending on the nature of the monomer and the conditions used during the deposition. The adhesion strength between the polymer film and the carbon fiber surface is strong. For instance, Cech et al.[26,27] managed to increase the adhesion strength between glass fibers and a polyester resin with a RF-plasma deposition of vinyltriethoxysilane, hexamethyldisiloxane, and tetravinylsilane monomers. In the case of carbon fibers, studies have entirely been focused on thermal curing so far. Jones' group[28−31] investigated a copolymerization of different systems such as acrylic acid-hexane, acrylic acid-1.7 octadiene, allyl alcohol-hexane, and allyl amine-octadiene to improve the adhesion strength with epoxy resins. Harris et al.[32] increased it as well by using acrylonitrile, hexamethylenetetramine, and o-diaminobenzene monomers. The plasma polymerization of styrene has been used for a polystyrene matrix.[33] Kang and Yoon[34] coated carbon fibers with a plasma polymer made from acetylene to tailor the interface properties of carbon fiber−vinyl ester composites.

In this study, carbon fibers were coated with a polymer film obtained by the plasma polymerization of maleic anhydride with conditions optimized in order to obtain the maximum retention rate. The surface of the coating was functionalized with acid anhydrides, vinyl, and thiol groups. The modifications of the fiber surface properties were related to the change in adhesion strength with an acrylate matrix cured by EB, measured by a micromechanical test derived from the pull-out test and well-adapted to our study. For comparison, specimens cured by an isothermal photopolymerization under ultraviolet (UV) light were also tested.

## II. MATERIALS AND METHODS

**II.A. Deposition of a Functionalized Plasma Polymer Coating at the Surface of the Fibers.** Toho Tenax Europe GmbH produced the intermediate modulus PAN-based Tenax IMS 5001 (12 k) carbon fibers used in this study. These fibers were surface treated by electrochemical oxidation and not sized. Their tensile modulus is 248 ± 20 GPa, their tensile strength 4.51 ± 0.51 GPa, and their elongation at break 1.6 ± 0.2%, according to some single filament tensile testing results reported elsewhere.[19]

Maleic anhydride was obtained in pellet form from Prolabo (purity of 99.5%) and was ground into a fine powder and loaded into a stoppered glass gas-delivery tube.

The deposit of the plasma polymer onto the surface of the fibers was carried out in an electrodeless cylindrical glass reactor (diameter = 6 cm, volume = 680 $cm^3$, base pressure = $5 \times 10^{-4}$ mbar, and with a leak rate better than $1.0 \times 10^{-10}$ kg $s^{-1}$) enclosed in a Faraday cage (Figure 1). Before every experiment, the reactor was thoroughly

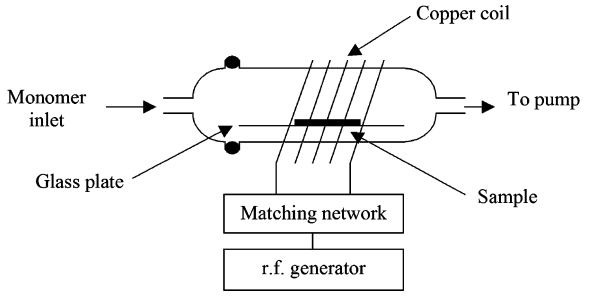


**Figure 1.** Schematic of the reactor used for plasma polymerization. Reproduced from ref 35 with permission from Elsevier, copyright 2005.

cleaned with detergent, rinsed with isopropanol, and dried in an oven. This was followed by a 30 min high-power (60 W) air plasma treatment. For XPS analysis, the surface treatment was applied to a single tow, which was spread as much as possible. For the manufacture of pull-out and wettability test specimens, separated single fibers were treated. These single fibers were glued on a rectangular paperboard frame which laid on two little glass cylinders, so that the entire surface of the single fibers was in contact with the plasma. The chamber was fitted with a gas inlet, a Pirani pressure gauge, a two-stage rotary pump (Edwards) connected to a liquid nitrogen cold trap, and an externally wound copper coil (diameter = 4 mm, 5 turns). No grease was used for the joints. An L-C matching network (Dressler, VM 1500 W-ICP) was used to match the output impedance of a 13.56 MHz Radio Frequency (RF) power supply (Dressler, Cesar 133) to the partially ionized gas load by minimizing the standing wave ratio of the transmitted power. An oscilloscope was used to monitor the pulse shape during electrical pulsing. The average power $P$ delivered to the system was calculated from the expression: $P = P_p[t_{on}/(t_{on} + t_{off})]$, where $P_p$ is the average continuous-wave power output and $t_{on}/(t_{on} + t_{off})$ is defined as the duty cycle (2% in our case). The electrical discharge parameters to get the maximum surface density of maleic anhydride groups were optimized by Siffer et al.[35] and were used in this study (Power 5 W, pulse on-time $t_{on}$ = 25 $\mu$s, pulse off-time $t_{off}$ = 1200 $\mu$s). Maleic anhydride vapor was introduced into the reaction chamber at a constant pressure of 20 Pa and with a flow rate of $1.6 \times 10^{-6}$ g $s^{-1}$. The time of deposition was 30 min. The RF generator was then switched off, and the monomer flow through the system was

maintained for another 2 min before venting up to atmospheric pressure.

The mechanism of maleic anhydride pulsed plasma polymerization was studied by Ryan et al.[36] and is reproduced in Figure 2.

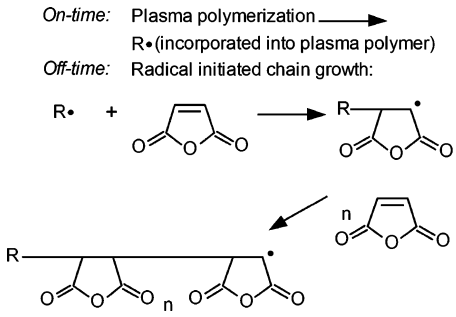


**Figure 2.** Mechanism of maleic anhydride plasma polymerization. Reproduced from ref 36 with permission from ACS publications, copyright 1996.

Since the matrix of the pull-out test specimens is an acrylate resin polymerizing through a radical polymerization, the anhydride groups were converted to pendant vinyl groups with the use of allylamine (Sigma-Aldrich, 99%), according to the mechanism[37,38] displayed in Figure 3.

To do so, allylamine, which was kept in a gas-delivery tube as well, was introduced in the reactor at a pressure of 100 Pa without exposing the coating to air, so that no hydrolysis of the anhydride group happened before the reaction with allylamine. Upon termination of exposure, the allylamine reservoir was isolated and the whole apparatus

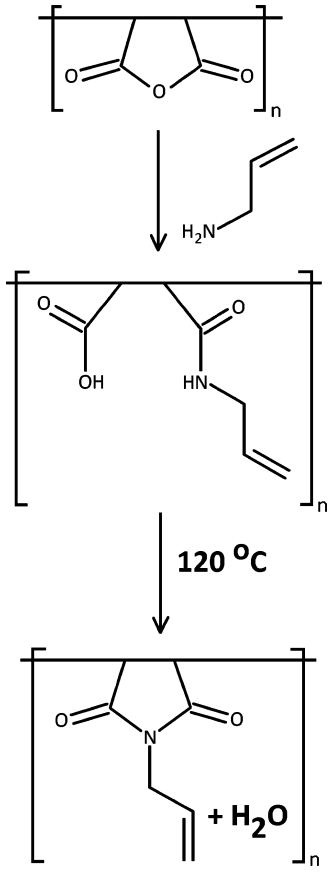


**Figure 3.** Grafting of pendant vinyl groups on the plasma polymer with allylamine.

pumped back down to the system base pressure. Then, the specimens were placed in an oven at 120 °C for 2 h in order to transform the amide groups into more stabilized cyclic imide groups (Figure 3).

It was mentioned in a previous study[24] that the grafting of thiol functionalities, which act as a chain transfer agent during the polymerization of the acrylate matrix, significantly increased the adhesion strength at the interface carbon fiber/acrylate resin cured by EB. The anhydride groups were then converted into thiol functionalities according to the mechanism reported in Figure 4.

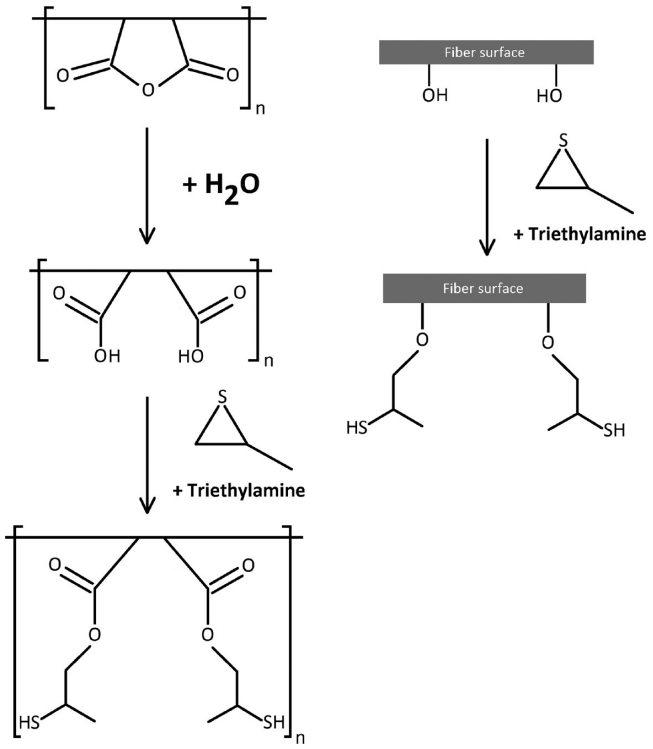


**Figure 4.** Grafting pendant thiol groups at the surface of the plasma polymer (left) and the pristine carbon fiber surface (right).

The protocol of such a grafting was performed as followed. The fibers coated with the plasma polymer were first left under ambient conditions overnight in order for the anhydride functionalities to be converted into carboxylic acid functionalities. Then, around 1 g of coated fibers was kept in a polypropylene bag and transferred in a flask containing 100 mL of toluene, propylene sulfide (Acros Organics, 99%) at a concentration of 1 mol $L^{-1}$, and triethylamine (Sigma-Aldrich, 99%) at a concentration of 0.1 mol $L^{-1}$. The boiling flask was connected to a condenser cooled with tap water. The solution was kept at 90 °C for 10 h and continuously stirred. The fibers were then washed with toluene first and with a mix of acetic acid and toluene (10:90) to remove traces of triethylamine. The fibers were then extracted in toluene with a Soxhlet extractor for 4 h and dried overnight in a vacuum oven at 40 °C and under a primary vacuum.

The fiber surface properties were characterized before and after surface treatment in terms of topography, surface chemistry, and surface energy. The adhesion strength at the interface was assessed by the measurement of the InterFacial Shear Strength (IFSS) with a test derived from the pull-out test.

**II.B. Analysis of the Surface Properties of the Fibers.** *II.B.1. Imaging at a Microscopic Scale.* The Philips 525 M Scanning Electron Microscope (SEM) was used in secondary electron mode. The acceleration voltage was 30 kV. No conductive coating was used for noncoated fibers, and a gold coating was used for fibers coated with a plasma polymer. MaxiView software was used for image analysis.

*II.B.2. Imaging at a Nanoscopic Scale.* Atomic force microscopy (AFM) imaging was performed using a Veeco D3000 Atomic Force Microscope in tapping mode and controlled by the software

**Table 1. XPS Peak Components Used for the Fitting of the C(1s), O(1s), and N(1s) Peaks, Analysis of the Noncoated Carbon Fiber Surface**

| C(1s) | | O(1s) | | N(1s) | |
|---|---|---|---|---|---|
| binding energy (eV) | component peak | binding energy (eV) | component peak | binding energy (eV) | component peak |
| 284.4 < < 284.6 | $Csp^2$ | 531.2 < < 531.4 | Ph═O (quinone), Ph−C═O | 398.4 < < 399.0 | pyridine |
| 284.9 < < 285.1 | $Csp^3$ | 532.0 < < 532.2 | C═O (ester, anhydride, amide), carboxylic acid | 399.4 < < 399.8 | amines, amides, nitriles |
| 284.8 < < 285.0 | C−COOR | 532.7 < < 532.9 | R−OH, C−O−C | 400.1 < < 400.7 | pyrrolidine, pyridone, urethane |
| 285.4 < < 285.6 | C−N | 533.5 < < 533.7 | Ph−OH, C−O (ester, anhydride) | 401.1 < < 401.7 | pyridinium, protonated N |
| 286.1 < < 286.4 | C−O−R, C≡N | 534.8 < < 535.2 | chemisorbed $H_2O$ | 403.7 < < 404.3 | shake up |
| 287.4 < < 287.6 | C═O | 536.2 < < 536.6 | physisorbed $H_2O$ | | |
| 288.3 < < 288.9 | COOR | 538.2 < < 538.6 | shake up | | |
| 290.1 < < 290.5 | physisorbed $H_20$ | | | | |
| 291.3 < < 291.7 | shake up | | | | |

**Table 2. XPS Peak Components Used for the Fitting of the C(1s), O(1s), N(1s), and S(2p) Peaks, Analysis of the Polymer Coating**

| C(1s) | | O(1s) | | N(1s) | | $S(2p_{3/2})-S(2p_{1/2})$ | |
|---|---|---|---|---|---|---|---|
| binding energy (eV) | component peak | binding energy (eV) | component peak | binding energy (eV) | component peak | binding energy (eV) | component peak |
| 284.9 < < 285.1 | $CH_x$ | 533.2 < < 533.6 | C═O | 399.9 < < 400.1 | N−$(C═O)_2$ (imine) | 163.5 < < 163.7−164.7 < < 164.9 | C−S−H |
| 286.1 < < 286.5 | C−COOR | 534.6 < < 535.0 | C−O | 401.9 < < 402.1 | protonated N | 168.1 < < 168.3−169.3 < < 169.5 | oxidized sulfur species (C−S−OH) |
| 287.3 < < 287.5 | C−O-R, C−S | | | | | | |
| 288.4 < < 288.8 | C═O, O−C−O, $(C═O)_2$-N (imine) | | | | | | |
| 290.0 < < 290.4 | O═C−O−C═O | | | | | | |

Nanoscope III. AFM tips with an aluminum reflex coating Tap300Al-G from Budget Sensors were used. Single fibers were deposited on some double-side adhesive tape that was covering the sample holder. The tip was carefully directed to the surface of the fiber during the approach step without touching the tape, thus avoiding a contamination of the tip that would affect the resolution of the images. Images of 1 $\mu$m × 1 $\mu$m were obtained.

*II.B.3. X-Ray Photoelectron Spectroscopy Analysis.* X-ray Photoelectron Spectroscopy (XPS) analysis of the carbon fibers was carried out with a SCIENTA SES-200 X-ray photoelectron spectrometer equipped with a conventional hemispherical analyzer that was operated in the Fixed Transmission Mode at constant pass energy of 100 eV. A monochromatic Al K$\alpha$ source (1486.6 eV, 14 kV, 30 mA) was used as the incident radiation. Photoemitted electrons were collected at a takeoff angle of 20° from the sample. The pressure was about $10^{-7}$ Pa. All binding energies were referenced to the C(1s) peak located at 284.6 eV. Instrumental sensitivity factors were taken as C(1s)/O(1s)/N(1s)/S(2p) equals 1.000:2.930:1.800:1.680. Core level spectra were fitted to the GL function (product of a Lorentzian by a Gaussian) by allowing some variation of the full-width-at-half-maximum (fwhm) using XPS CASA software. The component peaks used for the curve fitting of C(1s), O(1s), N(1s), and S(2p) peaks are reported in Table 1 for noncoated fibers and Table 2 for coated fibers, respectively. The O(1s) and peak N(1s) were fitted according to components suggested by other work.[39] The S(2p) peak was fitted according to components proposed by Vance et al.[40] A splitting between $S(2p_{3/2})$ and $S(2p_{1/2})$ of 1.2 eV and a branching ratio of 2:1 for their relative intensity were applied. The C(1s) peak fitting was performed so that the total area of all the oxy-carbonated components, all the nitro-carbonated components, and all the sulphuro-carbonated components could not be higher than the total area of the O(1s), the N(1s), and the S(2p) peaks, respectively.

*II.B.4. Determination of the Dispersive and Nondispersive Components of the Surface Energy by Wettability.* The two liquid phase method was used to measure the surface energy of the fibers and its dispersive and polar components. A single fiber was immersed at a constant speed successively in an alkane and in water, the alkane being superposed to the water. Five different alkanes were used: octane, nonane, decane, dodecane, and hexadecane. The electrobalance K14 from Krüss was used to measure the forces applied to the single fiber. The sensitivity was $10^{-6}$ g, and the speed of the displacement of the fiber was 1 mm $min^{-1}$. The method and the theory were described in detail by Schultz and Nardin[41] and in previous work as well.[19] The two liquid phase method is advantageous because it involves a dynamic wetting. An advancing contact angle and a hysteresis can be determined, which are representative of real surfaces, with different contact angles at equilibrium. The hysteresis assesses the influence of the roughness and the energy heterogeneity of the surface. This method does not require the value of the diameter of the fiber, which is very convenient when a surface treatment changes that value (abrasive treatment or coating of the fiber surface).

**II.C. EB and UV Curing of the Pull-Out Samples.** *II.C.1. Resin Ebecryl 600.* Ebecryl 600 from UCB Chemicals (now provided by Cytec) was used as the matrix. Its chemical structure is displayed in Figure 5. Before use, it was degassed under a vacuum. A temperature of 90 °C had to be set during the degassing in order to reduce its high viscosity (80 Pa s at 30 °C).

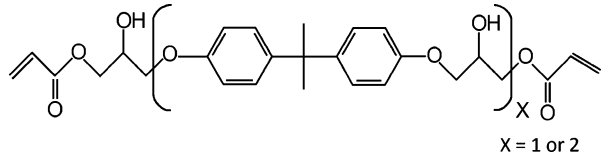


**Figure 5.** Molecular structure of the Ebecryl 600 monomer.


dx.doi.org/10.1021/am4045663 | ACS Appl. Mater. Interfaces 2014, 6, 1662−1674

*II.C.2. EB and UV Curing.* The conditions used for EB curing and UV curing have been extensively described elsewhere.[19,20] In both cases, the pull-out samples were cured under nitrogen, as oxygen is a strong inhibitor for radical polymerizations. EB curing was performed at EADS Astrium (UNIPOLIS facility, Saint-Médard en Jalles, France) with a total dose of 100 kGy. UV curing was conducted in the laboratory with a device that was specially designed (Figure 6). For

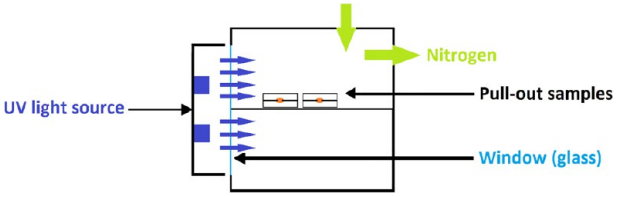


**Figure 6.** Device used for the UV curing of the pull-out test specimens. Reproduced from ref 21 with permission from Taylor & Francis, copyright 2013.

UV curing, Ebecryl 600 was mixed with 2.5 wt % of the photoinitiator Darocur 1173 (2-hydroxy 2-methyl propiophenone, provided by Ciba). The overall intensity of UV light was equal to 1 W $m^{-2}$. The reaction time was 2 h, and a supply of thermal energy enabled the pull-out specimens to be constantly exposed to a temperature of 90 °C during the curing.

*II.C.3. Assessment of the Fiber/Matrix Adhesion Strength by the Pull-Out Test.* The adhesion strength between the fibers and the resin was assessed by a micromechanical test derived from the single fiber pull-out test. A resin drop was deposited at the junction of two filaments (Figure 7). After curing, a tensile force was applied on the filaments by an Instron 4505 tensile test device equipped with a 10 N load cell. The filament having the shorter embedded length led to the pull-out phenomenon. The shear strength at a given embedded length was then calculated, considering that the maximum force $F_{max}$ measured during the test was the force applied when the debonding

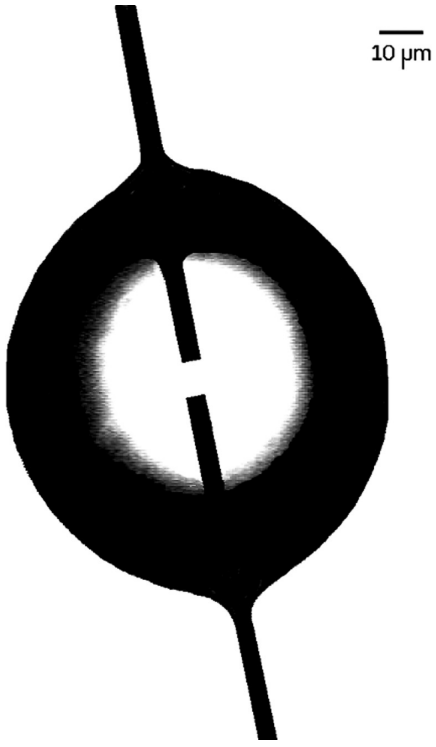


**Figure 7.** Architecture of the modified pull-out test specimens. Reproduced from ref 21 with permission from Taylor & Francis, copyright 2013.

of the interface occurred. The value of the shear strength was given by eq 1.

$$\tau = \frac{F_{max}}{2\pi r l_e} \quad (1)$$

with $r$ being the value of the radius of the fiber and $l_e$ the embedded length leading to the pull-out phenomenon.

Greszczuk's model was used for data reduction, leading to the estimation of the InterFacial Shear Strength (IFSS) by an extrapolation at an embedded length equal to zero.[42] The interfacial shear is related to the embedded length leading to the pull-out phenomenon according to eq 2:

$$\tau_{max} = \frac{\tau\alpha l_e}{\tanh(\alpha l_e)} \quad (2)$$

with $\alpha$ and the value of the interfacial shear strength $\tau_{max}$ being two constants that are characteristics of the considered fiber-matrix interface. For each fiber/matrix system, the IFSS was determined with at least 25 pull-out validated experiments. The values of $\alpha$ and $\tau_{max}$ were obtained by using the least-squares method for the fitting of the data with Greszczuk's model, using the software Origin. The embedded length $l_e$ was measured after pull-out with an optical microscope and the image analysis software ScnImage. A residual piece of resin at the point of entrance of the single fiber in the matrix droplet remained and enabled the measurement of the embedded length.[19]

## III. RESULTS AND DISCUSSION

**III.A. Characterization of the Fiber Surface at a Microscopic Scale.** SEM images of the surface of IMS 5001 carbon fibers before and after coating can be seen in Figure 8.

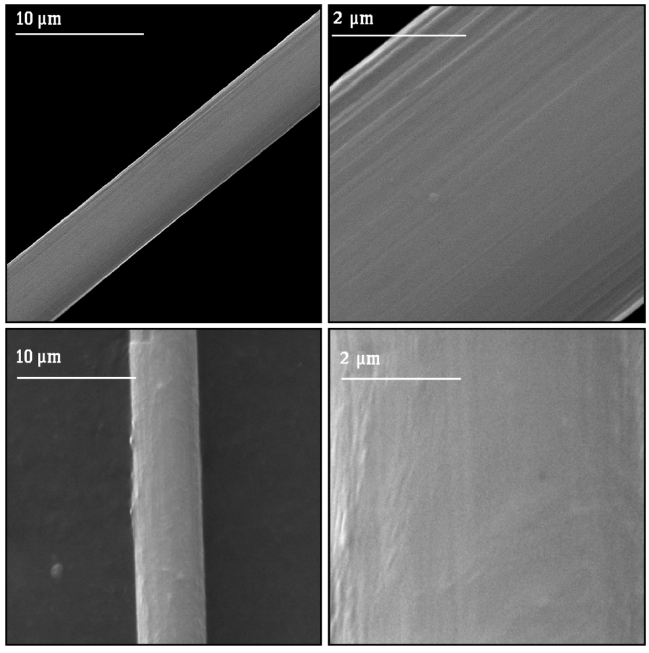


**Figure 8.** SEM images of the IMS 5001 fibers, noncoated (top) and coated by the plasma polymer (bottom).

When it comes to IMS 5001 fibers, typical grooves and ridges that are in the axis of the fiber can be seen. They were generated during the spinning process of the PAN precursor. After coating, those grooves can still be observed, but their depth appears to be diminished. The generation of a film at the surface of the fibers is obvious, and the entire surface is covered. Nevertheless, it appears that the surface of the coating is not perfectly even, since a few aggregates can be observed. The

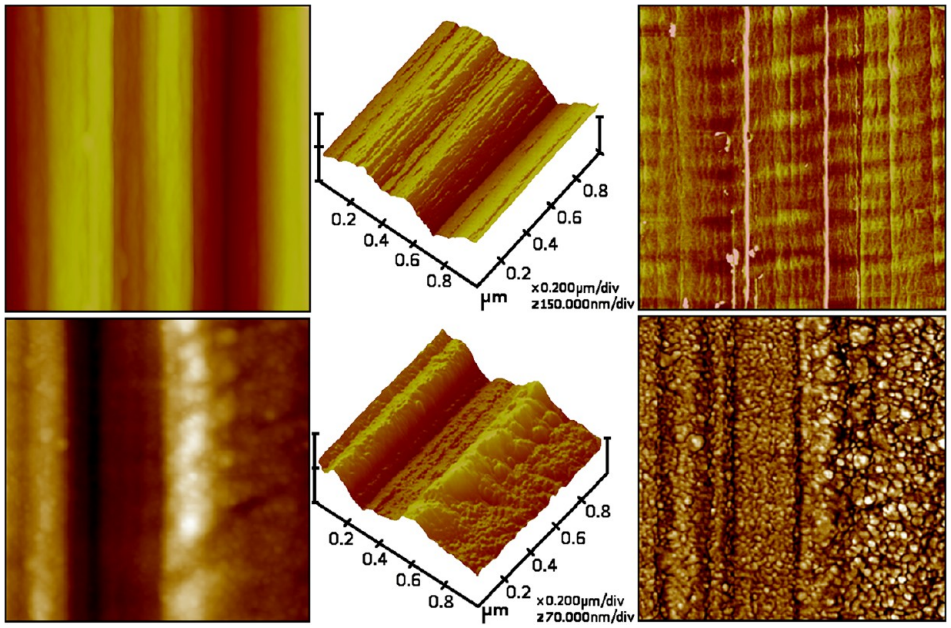


**Figure 9.** AFM images of the surface of IMS 5001 fibers, noncoated (up) and coated by the plasma polymer (bottom). Left, 2D-topography; middle, 3D-topography; right, phase contrast. Part of this figure is reproduced from ref 19 with permission from Elsevier, copyright 2012.

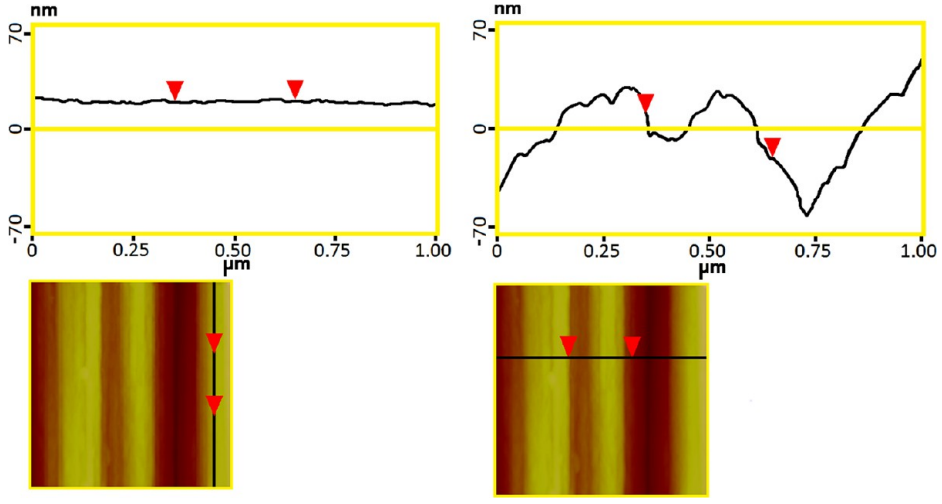


**Figure 10.** Surface topography of noncoated IMS 5001 fibers, along the fiber axis (left) and perpendicularly to the fiber axis (right). Reproduced from ref 19 with permission from Elsevier, copyright 2012.

diameter of 20 different single fibers was determined by image analysis and the average value was found to be 5.4 ± 0.3 $\mu$m before and 5.6 ± 0.3 $\mu$m after the polymer coating, so no significant difference was noticed at the micrometric scale, in accordance with the value of the coating thickness that was expected (around 16 nm). In order to obtain more details about the structure of the coating at the nanometric scale, AFM observations were conducted as well.

**III.B. Characterization of the Fiber Surface at a Nanoscopic Scale.** Images of IMS 5001 fiber surfaces with and without coating and obtained with the tapping mode are displayed in Figure 9. For the sake of clarity, the 3D equivalent of the 2D topography images is given, as well as the phase contrast image. As reported in a previous study,[19] the surface of IMS 5001 fibers is made of a primary structure constituted of the grooves and ridges oriented in the axis of the fiber and observed in the SEM pictures. As shown by a profile of the surface obtained perpendicularly to the fiber axis, the depth of the grooves is around 70 nm, and their thickness is around 200−250 nm (Figure 10). After the plasma polymerization treatment, a similar profile of the surface gave a value of 50−60 nm for the depth of the grooves (Figure 11). Taking into consideration that there may be a slight variation from groove to groove, the AFM characterization showed that the coating was spread relatively evenly on the fibers, as it did not fill up the grooves. When using the same conditions of deposition with a silicon wafer as the support, Siffer et al.[35] reported that the thickness of the polymer coating was 16 nm using ellipsometry, and this was confirmed by leaving a silicon wafer close to the fibers in the plasma chamber. In addition, the phase contrast image (Figure 9) revealed a very typical structure of the polymer film. Indeed, it was made of packed circular-shaped grains with a 20−30 nm diameter. Siffer et al.[35] obtained exactly the same structure with a deposition on a silicon wafer using

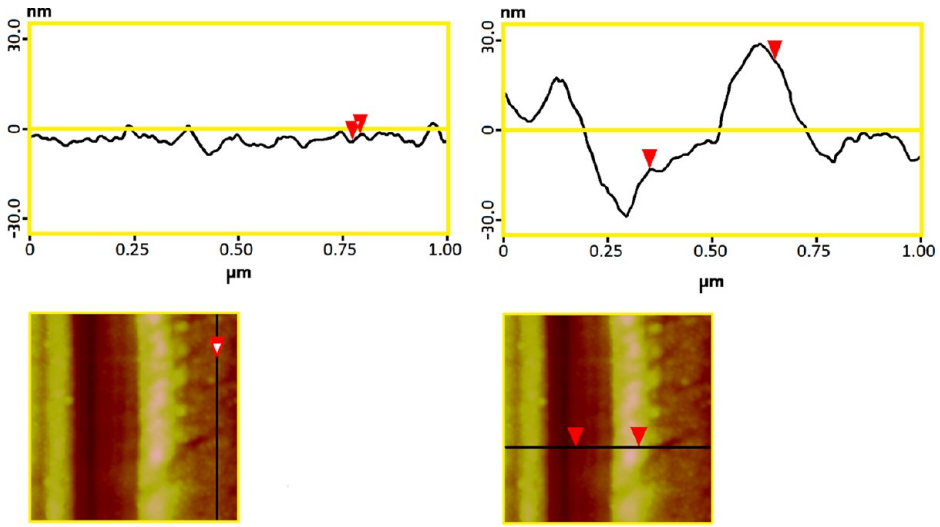


**Figure 11.** Surface topography of the plasma polymer coated IMS 5001 fibers, along the fiber axis (left) and perpendicularly to the fiber axis (right).

the same conditions of deposition. That phase contrast image also confirmed that the polymer film potentially covered the whole fiber surface.

For both coated and noncoated fibers, a secondary structure made of smaller grooves was superposed to the primary structure. Considering the surface of the ridges in the case of noncoated fibers, it was very smooth, with amplitudes that were below 3 nm (Figure 10—along the fiber axis). The amplitudes of the roughness generated by the grains that constituted the structure of the polymer coating were up to 10 nm (Figure 11—along the fiber axis). Compared to noncoated fibers, this structure generates some extra mechanical interlocking with the acrylate matrix. Indeed, Gao et al.[43] claimed that the fiber surface contributes to interfacial adhesion through mechanical interlocking only if its roughness is lower than a few tens of nanometers. Since the level of interfacial adhesion strength is also determined by the surface energy and the surface chemistry of the fibers, these properties were characterized as well.

**III.C. Analysis of the Surface Chemistry by X-Ray Photoelectron Spectroscopy.** The survey spectra of pristine IMS 5001 fibers and coated IMS 5001 fibers, with the functionalization in vinyl and thiol groups, are presented in Figure 12. The corresponding elemental analysis is reported in Table 3. The fitting of high resolution O(1s), N(1s), and S(2p) spectra is shown in Figure 13, and the relative area of each component in the fitting of C(1s), O(1s), N(1s), and S(2p) peaks can be found in Table 4.

The surface chemistry of IMS 5001 carbon fibers was constituted of carboxylic acid, ether, alcohol, quinone, and lactone functionalities when considering the oxy-carbonated functional groups. Nitro-carbonated functionalities were made of amines, amides, and nitrogen incorporated in the fiber structure as a remaining precursor (aromatic functionalities like pyridine, pyrrolidine, pyridone).

The concentration in oxygen increased from 15% to 30% after coating by plasma polymerization of maleic anhydride. The peak corresponding to nitrogen disappeared, which confirmed that the entire original fiber surface was evenly covered by a coating with a thickness that was greater than the thickness probed by XPS (around 3−5 nm). The fitting of the C(1s) peak confirmed that the surface chemistry of the plasma polymer was constituted mainly by maleic anhydride functionalities and that the maleic anhydride group retention was 30%, which is in accordance with the 32% obtained with the same deposition conditions on a silicon wafer.[35] The fitting of the O(1s) peak also confirmed relative areas very close to 2/3 and 1/3 and corresponding to C═O and C−O covalent bonds, respectively. This corresponds to the structure of the plasma polymer presented in Figure 3.

After the reaction with allylamine and the generation of cyclic imide groups, nitrogen was detected, and its atomic concentration was 5%. The fitting of the N(1s) peak and the C(1s) peak confirmed the generation of an imine compound, with the components located at 400.0 eV and at 288.6 eV, respectively. Particularly, the fitting of the N(1s) peak showed that a small portion of the imine functionalities underwent acid−base interactions with adjacent carboxylic acid functionalities to form protonated nitrogen species. Those carboxylic acid functionalities were generated during the plasma polymerization of maleic anhydride and also by hydrolysis of the maleic anhydride functionalities that did not react with allylamine (exposure of the sample to moisture).

The reaction of the coating with propylene sulfide was confirmed by the generation of a peak corresponding to sulfur, which was found to be at a concentration of 5%. Traces of nitrogen could be detected as well, which suggests that the sample may have not been covered evenly by the coating or that a part of the coating was detached from the fiber by toluene during the reaction with propylene sulfide. But this phenomena was limited, as the component peak corresponding to C($sp^2$) in the fitting of the C(1s) peak was low. As reported in a previous study, the grafted thiol functionalities are oxidized rapidly when they are stored under ambient conditions, which is highlighted by the fitting of the S(2p) peak.

**III.D. Measurement of the Surface Energy and Its Dispersive and Polar Components.** The dispersive and polar components of the surface energy of IMS 5001 fibers, with and without the three different types of coatings, can be found in Table 5 (Figure 14). Due to a large scatter in the results, no significant difference was measured between the dispersive components of the different systems, all values being around 30 mJ $m^{-2}$. A clear difference was noticed regarding the polar component. A significant increase was measured after the coating with maleic anhydride, which is the direct consequence

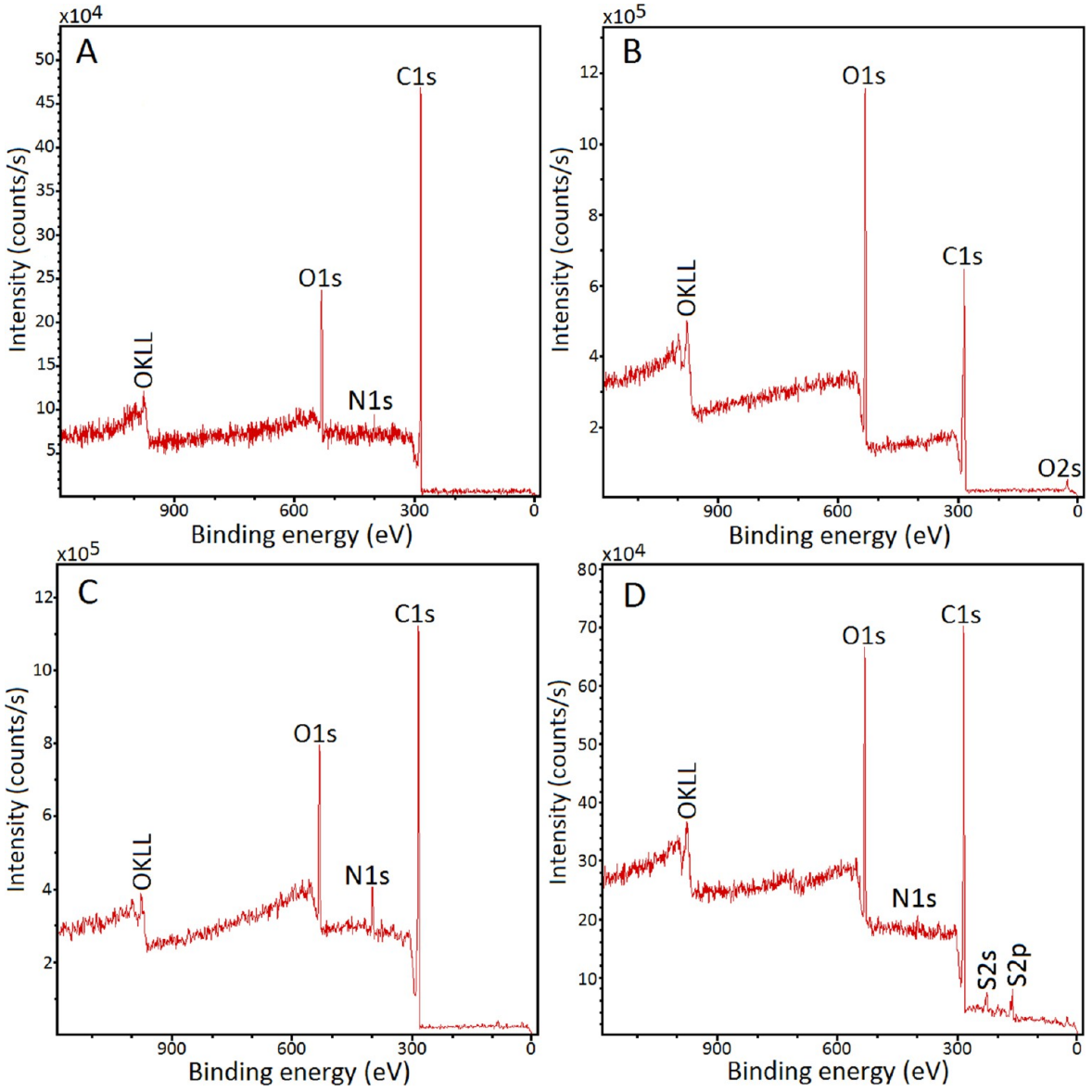


**Figure 12.** XPS survey spectra of (A) pristine IMS 5001 fibers, (B) IMS 5001 fibers coated with the maleic anhydride plasma polymer, (C) IMS 5001 fibers coated with a plasma polymer functionalized with vinyl groups, and (D) IMS 5001 fibers coated with a plasma polymer functionalized with thiol groups.

**Table 3. XPS Elemental Analysis of the Carbon Fiber Surface before and after Coating**

| sample reference | % C | % O | % N | % S |
|---|---|---|---|---|
| IMS 5001 fibers | 83 | 15 | 2 | 0 |
| IMS 5001 fibers + maleic anhydride plasma polymer | 70 | 30 | 0 | 0 |
| IMS 5001 fibers + plasma polymer functionalized with vinyl groups | 81 | 14 | 5 | 0 |
| IMS 5001 fibers + plasma polymer functionalized with thiol groups | 74 | 20 | 1 | 5 |

of the generation of a high surface density of anhydride groups. The anhydride groups are hydrophilic, that is why the advancing contact angle measured with water was 17°, whereas it was only 60° with noncoated IMS 5001 fibers. After functionalization of the coating with pendant vinyl groups, the relative concentration of oxygen decreased, which participated in lowering the value of the polar component of the free surface energy. The advancing contact angle with water was only 80°. After functionalization with thiol groups, the values did not change significantly (advancing contact angle of 37°). An improvement of wettability of the fiber by model liquids does not guarantee that the wettability by the acrylate resin is significantly better, but it can be expected that the increase of the polar component of the surface energy may facilitate the wetting of the fiber by the matrix during the manufacture of the composite, because of the hydroxyl groups existing in the acrylate monomer. The surface topography changed as well, but since no information about the wettability of the fiber by the resin is known, it is not clear at this stage if the topography of the polymer coating has a positive or negative influence. Last, a good wetting of the fiber by the resin is a necessary but not sufficient condition for a good interfacial adhesion.

**III.E. Assessment of the Adhesion Strength by a Modified Pull-Out Test.** It was shown elsewhere[19] that the conversion fraction of the matrix in the bulk was found to be 0.75 for EB curing and 0.78 for UV curing, respectively. Those


dx.doi.org/10.1021/am4045663 | ACS Appl. Mater. Interfaces 2014, 6, 1662−1674

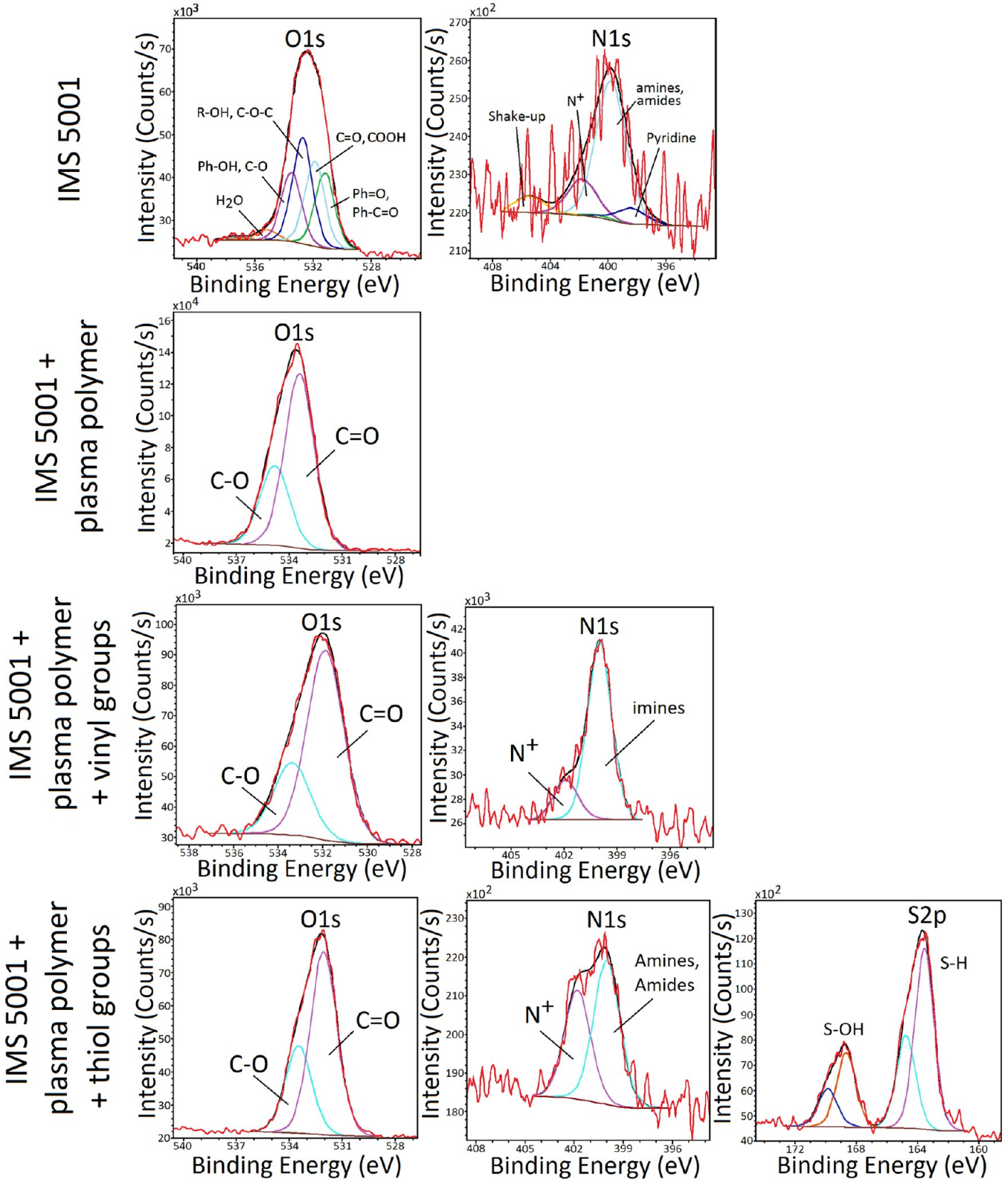


**Figure 13.** XPS core spectra, pristine and coated IMS 5001 fibers. For the sake of clarity, only the spectra corresponding to the heteroatoms are given.

values indicate that the cure of the matrix was complete in the bulk. Also, Krzeminski et al.[44,45] proved that, if the value of the conversion fraction was the same, the mechanisms generating the molecular structure of the polymerized Ebecryl 600 in the bulk did not depend on the initiation mechanism, the curing temperature, and the polymerization time scale. The only explanation for the same carbon fiber/matrix system with a similar conversion fraction to show different adhesion strengths is a difference in the mechanical properties at the interphase, that is to say a difference in the structure of the matrix close to

**Table 4. Relative Area of Each of the Components in the Fitting of C(1s), O(1s), N(1s), and S(2p) XPS Peaks, in Percentage of the Total Area of the Peak**

| | C(1s) | | | | | | | | O(1s) | | | | | | | N(1s) | | |
|---|---|---|---|---|---|---|---|---|---|---|---|---|---|---|---|---|---|---|
| IMS 5001 | $Csp^2$ | $Csp^3$ | C–O–R | C=O | COOR | C–COOR | C–N | Ph=O, Ph–C=O | C=O | Ph–OH, C–O | R–OH, C–O–C | $H_2O$ | pyridine | nitriles, amines, amides | pyridone, urethane | pyridinium, protonated N | | |
| | 76 | 4 | 5 | 3 | 5 | 5 | 2 | 32 | 12 | 10 | 44 | 2 | 8 | 68 | 1 | 23 | | |
| IMS 5001 + maleic anhydride | C(1s) | | | | | | | | | | | | O(1s) | | | | | |
| | $CH_x$ | | C–C(O)–O | | C–OR | | | C=O, O–C–O | | | O=C–O–C=O | | C=O | | C–O | | | |
| | 22 | | 36 | | 12 | | | 2 | | | 28 | | 69 | | 31 | | | |
| IMS 5001 + plasma polymer + vinyl | C(1s) | | | | | | | | | | | | O(1s) | | | N(1s) | | |
| | $CH_x$ | | C–COOR | | C–OR | | $(C=O)_2$-N | | C=O | | COOR | | C=O | | C–O | protonated N | | |
| | 73 | | 3 | | 10 | | 7 | | 4 | | 3 | | 72 | | 28 | 18 | | |
| IMS 5001 + plasma polymer + thiol | C(1s) | | | | | | | | | | | | O(1s) | N(1s) | | S(2p) | | |
| | $Csp^2$ | $CH_x$, $Csp^3$ | C–COOR | | C–N | | C–OR, C–S | | C=O | | COOR | | C=O | C–O | pyridinium | nitrile, amines amides | S–H | S–OH |
| | 8 | 56 | 10 | | 3 | | 14 | | 3 | | 6 | | 68 | 32 | 43 | 57 | 70 | 30 |

**Table 5. Polar and Dispersive Components of the Surface Energy of Noncoated and Coated IMS 5001 Fibers**

| | $\gamma^D$ (mJ m$^{-2}$) | $\gamma^P$ (mJ m$^{-2}$) |
|---|---|---|
| IMS 5001 fibers | 37 ± 15 | 33 ± 14 |
| IMS 5001 fibers + maleic anhydride | 29 ± 13 | 57 ± 9 |
| IMS 5001 fibers + plasma polymer + vinyl | 36 ± 17 | 19 ± 4 |
| IMS 5001 fibers + plasma polymer + thiol | 24 ± 14 | 49 ± 10 |

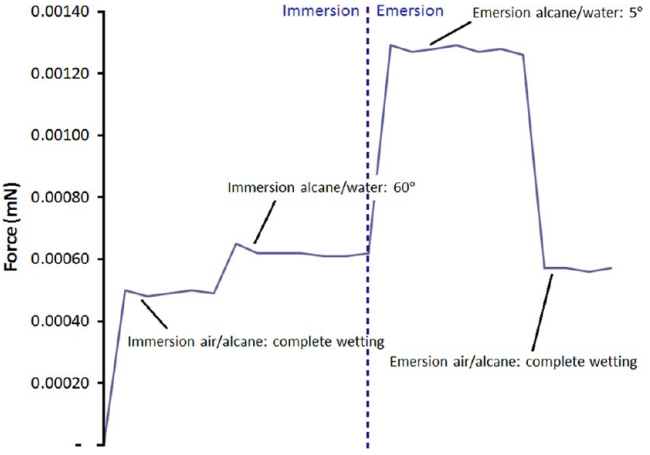


**Figure 14.** Two liquid phase method analysis (dodecane–water system) of IMS 5001 fibers.

the surface of the fiber and/or in the interactions existing in this interphase.

The determination of the IFSS by Greszczuk's approach applied to our single fiber pull-out test is illustrated in Figure 15

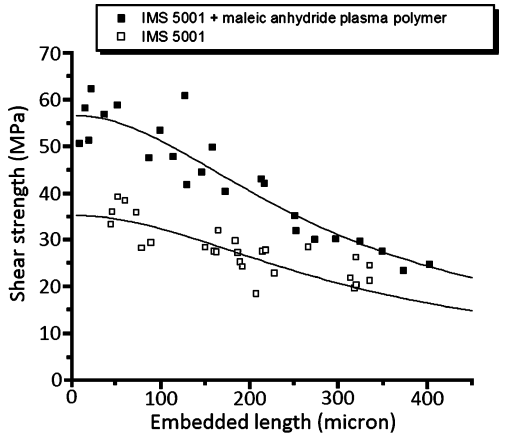


**Figure 15.** IMS 5001-Ebercyl 600 interface, before and after the coating with the maleic anhydride plasma polymer, EB curing. Reduction of the data obtained with the pull-out test using Greszczuk's model.

for two experimental cases. The values of the IFSS are respectively 35 ± 2 MPa for the pristine IMS 5001 fibers and 57 ± 2 MPa for the fibers coated with a maleic anhydride plasma polymer, that is to say an increase of 63% (Table 6). Insulating the inhibiting surface of the carbon fibers with a polymer covalently bonded to the carbon fiber definitely had a positive influence on the adhesion strength. This insulating polymeric layer can prevent electronic losses in the conductive carbon fibers during EB curing. When this polymer layer exhibited compatible chemical functionalities, that is to say


dx.doi.org/10.1021/am4045663 | ACS Appl. Mater. Interfaces 2014, 6, 1662–1674

**Table 6. IFSS Values Obtained with the Modified Pull-Out Test**

| | | IFSS (MPa) | |
|---|---|---|---|
| | fiber surface treatment | UV curing | EB curing |
| present results | IMS 5001 | 49 ± 3 | 35 ± 2 |
| | IMS 5001 + maleic anhydride | 72 ± 4 | 57 ± 2 |
| | IMS 5001 + plasma polymer + vinyl | 68 ± 2 | 74 ± 5 |
| | IMS 5001 + plasma polymer + thiol | 74 ± 3 | 78 ± 8 |
| previous results | IMS 5000 + nitric acid oxidation[20] | 56 ± 3 | 40 ± 3 |
| | IMS 5000 + $O_2$ plasma oxidation[21] | 65 ± 4 | 37 ± 3 |
| | IMS 5001 + acrylate groups (coupling agent grafting on fiber surface)[23] | 61 ± 4 | 65 ± 3 |
| | IMS 5001 + thiol groups (coupling agent grafting on fiber surface)[24] | 58 ± 3 | |
| | fiber surface treatment | thermal curing | |
| | IMS 5001[18] | 82 ± 3 | |

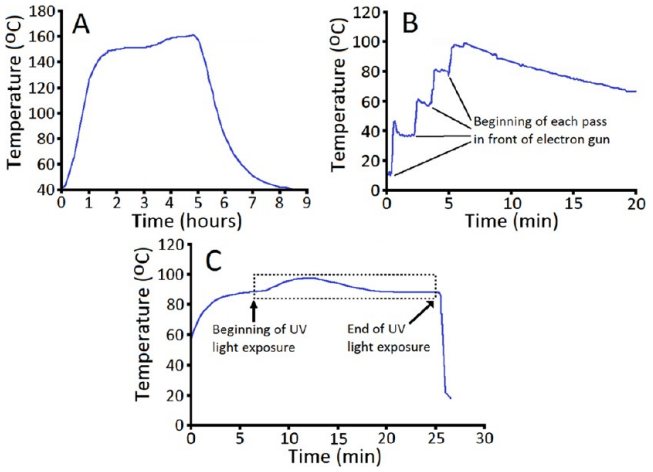


**Figure 16.** Typical thermal history of the matrix during the cure of carbon fiber−Ebecryl 600 composites with (A) thermal curing, (B) EB curing, and (C) UV curing.

chemical functionalities generating covalent bonding with the matrix during its polymerization, further improvement was obtained. Indeed, when that polymer coating was functionalized with pendant vinyl groups or pendant thiol groups, the adhesion strength increased to 74 ± 5 MPa (+111%) and 78 ± 8 MPa (+123%), respectively. These results are not correlated with those concerning the surface energy of the fibers (Table 5), indicating that strong interfacial interactions, like chemical covalent bonds, have to be considered in addition to physical interactions (i.e., van der Waals interactions). Such improvements are very sharp in comparison to the enhancements that were generated by surface oxidation treatments (nitric acid oxidation[20] and $O_2$ plasma[21]) or the grafting of the same functionalities directly on the carbon fiber surface with coupling agents.[23,24] This can be explained for several reasons that may have produced a synergetic effect. First, the surface density of those functionalities was higher when the grafting was made on the plasma polymer, as quantified by XPS analysis. Second, the carbon fiber was shielded from the matrix, so all the functionalities having a negative influence (phenols and amines, as shown by Ponsaud[46]) on the polymerization of the matrix in the vicinity of the fiber surface were ineffective. Third, the cure volume shrinkage of the matrix is around 4.5−5.0%, and this can have a negative influence on interfacial adhesion when it is 5.0% or higher.[17] Inserting a polymer layer with a high retention rate of anhydride functionalities can provide a buffer effect and counteract the stress generated at the interface by the cure volume shrinkage of the matrix. The thickness of that layer is an important parameter,[25] but it has not been optimized for this study, and further improvement of the adhesion strength may be obtained. A slightly higher IFSS was obtained when the length of the backbone of the coupling agent was longer ("grafting from" method).

In order to compare the level of adhesion obtained with the different curing processes, it is important to take into consideration the thermal history of the sample associated with each process, as shown in Figure 16. The thermal profiles presented here correspond to "real" composite plates with a fiber volume concentration of 60%. Of course, due to the shape of the pull-out samples, the thermal energy transfer to the surrounding environment may be slightly different, especially for EB curing, since the atmosphere is at room temperature. The thermal profile corresponding to UV curing is related to a thin film of the same resin cured under the same conditions as for the pull-out specimens, so it can be considered that the thermal history is pretty similar (that is to say an isothermal polymerization). When comparing the IFSS values between EB and UV curing, it can be concluded that a polymer layer functionalized with compatible groups gives the same level of adhesion strength with both curing modes (it was also the case with the grafting of acrylate groups directly on the carbon fiber surface[23]). The IFSS values obtained with oxidative surface treatments were systematically higher with UV curing, because optimal physical interactions could take place, due to a slow kinetics of polymerization. This could explain also why a higher IFSS was obtained with UV curing when the maleic anhydride plasma polymer was not modified. Indeed, a high density of hydrogen interactions between the anhydride groups and the hydroxyl groups of the Ebecryl 600 monomer is possible, and a slow kinetics of polymerization may be favorable for such interactions to be optimized.

The IFSS values obtained with the plasma polymer functionalized with vinyl and thiol groups were very close to the value corresponding to a composite cured by a thermal process (with tert-butyl peroxide as the initiator of the polymerization; Figure 17). In the case of a thermal cure, previous work[18,38] showed that the high values of IFSS were due to the generation of covalent bonding when carboxylic acids located at the carbon fiber surface were degraded by the thermal treatment (which did not happen with UV curing or EB curing because the necessary temperature around 150−160 °C was not reached) and also by the generation of covalent bonding by a reaction of pendant amine groups with the acrylate groups of the monomers by an aza-Michael reaction, potentially even before the polymerization of the matrix started. Also, the thermal history of the sample during the cure gives favorable conditions for the generation of optimized physical interactions at the interface (hydrogen bonding).

In comparison to thermal curing, almost identical adhesion strengths were obtained, therefore solving the interfacial adhesion issues in carbon fiber composites cured by EB. To the best of our knowledge, this is the first time that such high levels of IFSS have been reported in the case of carbon fiber composites cured by EB. The association of this type of carbon fiber surface treatment with a reinforced acrylate matrix should result in enhanced mechanical properties (fracture resistance

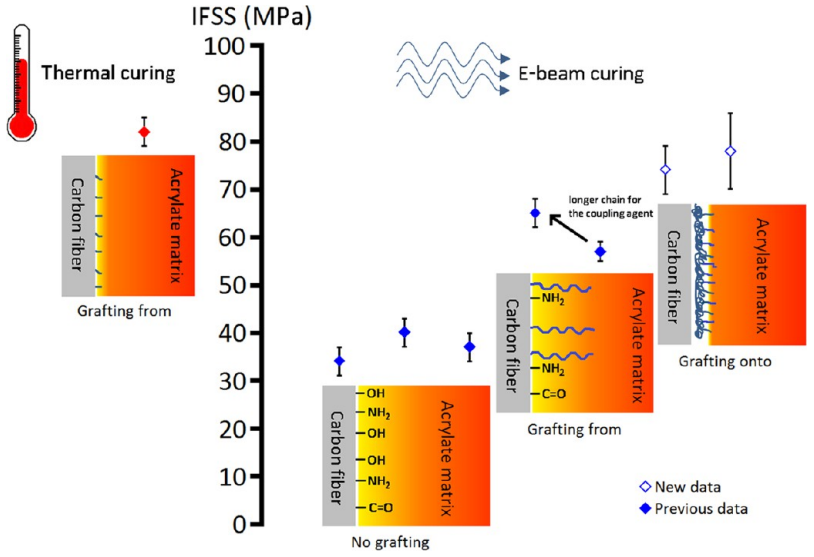


**Figure 17.** Summary of the mechanisms taking place in the different surface treatments investigated for the improvement of adhesion strength in carbon fiber−acrylate composites cured by EB and thermal treatment.

and transverse properties). One challenge is the scaling-up of the plasma polymerization process in a continuous surface treatment meeting industrial practices. The coating of the carbon fiber with a plasma polymer having thiol groups can also be obtained in one step by the use of an allylmercaptan monomer.[47] Further work needs to be focused on the development of this technology.

## IV. CONCLUSIONS

In this study, the coating of carbon fiber surfaces by a plasma polymerization technique was found to be a very efficient way to improve interfacial mechanical properties in composites cured by an electron beam. A shielding of the fiber surface by a polymer layer and the functionalization of this polymer layer with functional groups that can generate covalent bonding during the cure were two necessary conditions that had to be filled in order to obtain high levels of adhesion strength. The combination of a polymer layer covalently bonded to both the carbon fiber surface and the matrix appeared to be an optimized interphase. Overall, it was clear that the thermal history of the sample during the cure was a major parameter determining the level of adhesion strength. Because the kinetics of the polymerization is rapid and the rise of temperature of the sample is limited during EB curing, the carbon fiber surface properties had to be modified to be compatible with such processing parameters.

## AUTHOR INFORMATION

### Corresponding Author

*Fax: (+33) 389608799. E-mail: vautard@hotmail.fr, vautard@msu.edu.

### Notes

The authors declare no competing financial interest.

## ACKNOWLEDGMENTS

ANRT (Association Nationale de la Recherche et de la Technologie) is gratefully acknowledged for the Ph.D. grants assigned to F. Vautard. The gratitude of the authors is fully expressed to S. Ollivier who participated in the characterization of the surface properties of the fibers (AFM) and to P. Ponsaud (Laboratoire de Chimie Organique et Macromoléculaire, Université de Lille, France) and Professor X. Coqueret (Institut de Chimie Moléculaire de Reims, Université de Reims Champagne Ardenne, France) regarding their contribution to this work. A. Ponche from IS2M is sincerely thanked for fruitful discussion about XPS analysis. X. Dupont and M. Frayssines from EADS Astrium are also acknowledged for conducting the electron beam curing UNIPOLIS facility. Ciba is sincerely thanked for supplying the photoinitiator used in this study.

## REFERENCES

(1) Singh, A.; Saunders, C. In *Radiation processing of polymers*; Singh, A., Silvermann, J., Eds.; Hanser Publishers: New York, 1992; pp 187−203.
(2) Raghavan, J. *Composites, Part A* **2009**, *40*, 300−308.
(3) Sands, J. M.; Fink, B. K.; Mcknight, S. H.; Newton, C. H.; Gillepsie, J. W., Jr.; Palmese, G. R. *Clean Technol. Environ. Policy* **2001**, *2*, 228−235.
(4) Sparado, G.; Alessi, S.; Dispenza, C.; Sabatino, M. A.; Pitarresi, G.; Tumino, D.; Przbytniak, G. *Radiat. Phys. Chem.* **2014**, *94*, 14−17.
(5) Janke, C. J.; Dorsey, G. F.; Havens, S. J.; Lopata, V. J. In Toughened epoxy resins cured by electron beam radiation. *Proceedings of the 28th International SAMPE Technical Conference*, Seattle, WA, USA, Nov. 4−7, 1996; Society for the Advancement of Material and Process Engineering (SAMPE): Covina, CA, 1996.
(6) Defoort, B.; Chauray, E.; Ponsaud, P.; Coqueret, X. In Improvement of mechanical properties of acrylate based EB cured composite materials. *Proceedings of the International SAMPE Technical Conference*, Seattle, WA, Oct. 31−Nov 3, 2005; Society for the Advancement of Material and Process Engineering (SAMPE): Covina, CA, 2005.
(7) Kreminski, M.; Defoort, B.; Coqueret, X. In Nanoscale toughening matrices cured under electron beam activation for high performance composite applications. *Proceedings of the International SAMPE conference*, Seattle (WA), USA, May 17−20, 2010; Society for the Advancement of Material and Process Engineering (SAMPE): Covina, CA, 2010.
(8) Vautard, F.; Fioux, P.; Vidal, L.; Schultz, J.; Nardin, M.; Defoort, B. *Composites, Part A* **2011**, *42*, 859−867.
(9) Nardin, M.; Asloun, E. M.; Schultz, J. In *Controlled Interphases in Composite Materials*; Ishida, H., Ed.; Elsevier: New York, 1990; pp 285−293.
(10) Jennings, C. W. *J. Adhes.* **1972**, *4*, 25−38.

(11) Raghavendran, V. K.; Drzal, L. T.; Askeland, P. *J. Adhes.* **2002**, *16*, 1283−1306.
(12) Owens, D. K.; Went, R. C. *J. Appl. Polym. Sci.* **1969**, *13*, 1741−1747.
(13) Fowkes, F. M. *J. Adhes. Sci. Technol.* **1987**, *1*, 7−27.
(14) Hook, K. J.; Agrawal, R. K.; Drzal, L. T. *J. Adhes.* **1990**, *32*, 157−170.
(15) Pastor-Blas, M. M.; Sanchez-Adsuar, M. S.; Martin-Martinez, J. M. *J. Adhes.* **1995**, *50*, 191−210.
(16) Paiva, M. C.; Nardin, M.; Bernardo, C. A.; Schultz, J. *Compos. Sci. Technol.* **1997**, *57*, 839−843.
(17) Vautard, F.; Xu, L.; Drzal, L. T. In *Major accomplishments in composite materials and sandwiches structures*; Daniel, I. M., Gdoutos, E. E., Rajapakse, Y. D. S., Eds.; SpringerLink: Netherlands, 2010; pp 27−50.
(18) Vautard, F.; Ozcan, S.; Poland, L.; Nardin, M.; Meyer, H. *Composites, Part A* **2013**, *45*, 162−172.
(19) Vautard, F.; Fioux, P.; Vidal, L.; Schultz, J.; Nardin, M.; Defoort, B. *Int. J. Adhes. Adhes.* **2012**, *34*, 93−106.
(20) Vautard, F.; Fioux, P.; Vidal, L.; Dentzer, J.; Schultz, J.; Nardin, M.; Defoort, B. *Surf. Interface Anal.* **2013**, *45*, 722−741.
(21) Vautard, F.; Fioux, P.; Vidal, L.; Dentzer, J.; Schultz, J.; Nardin, M.; Defoort, B. *J. Adhes.* **2013**, *89*, 460−485.
(22) Bao, J.; Li, Y.; Zhong, X.; Chen, X. *Adv. Compos. Lett.* **2011**, *20*, 149−153.
(23) Vautard, F.; Fioux, P.; Vidal, L.; Schultz, J.; Nardin, M.; Defoort, B. *J. Adhes. Sci. Technol.* **2013**, *27*, 2352−2366.
(24) Vautard, F.; Fioux, P.; Schultz, J.; Nardin, M.; Defoort, B. *Appl. Surf. Sci.* **2013**, *286*, 12−21.
(25) Vautard, F., Drzal, L. T. In Carbon fiber-vinyl ester interfacial adhesion improvement by the use of a reactive epoxy coating. *Proceedings of the 17th International Conference on Composite Materials (ICCM-17)*, Edinburgh, Scotland, Jul. 27−31, 2009.
(26) Balkova, R.; Jancar, J.; Cech, V. *Compos. Sci. Technol.* **2009**, *69*, 2485−2490.
(27) Cech, V. *Compos. Interfaces* **2007**, *14*, 321−334.
(28) Kettle, A. P.; Beck, A. J.; O'Toole, L.; Jones, F. R. *Compos. Sci. Technol.* **1997**, *57*, 1023−1032.
(29) Lopattananon, N.; Kettle, A. P.; Tripathi, D.; Beck, A. J.; Duval, E.; France, R. M .; Short, R. D.; Jones, F. R. *Composites, Part A* **1999**, *30*, 49−57.
(30) Kettle, A. P.; Jones, F. R.; Alexander, M. R.; Short, R. D.; Stollenwerk, M.; Zabold, J.; Michaeli, W.; Wu, W.; Jacobs, E.; Verpoest, I. *Composites, Part A* **1998**, *29A*, 241−250.
(31) Lopattananon, N.; Hayes, S. A.; Jones, F. R. *J. Adhes.* **2002**, *78*, 313−350.
(32) Harris, B.; Braddell, O. G.; Lefebvre, C.; Verbist, J. *Plast., Rubber Compos. Process. Appl.* **1992**, *18*, 221−240.
(33) Yuan, L. Y.; Shyu, S. S.; Lai, J. Y. *J. Appl. Polym. Sci.* **1991**, *42*, 2525−2534.
(34) Kang, H. M.; Yoon, T. H. *J. Adhes. Sci. Technol.* **2002**, *16*, 1809−1823.
(35) Siffer, F.; Ponche, A.; Fioux, P.; Schultz, J.; Roucoules, V. *Anal. Chim. Acta* **2005**, *539*, 289−299.
(36) Ryan, M. E.; Hynes, A. M.; Badyal, J. P. S. *Chem. Mater.* **1996**, *8*, 37−42.
(37) Roucoules, V.; Ponche, A.; Siffer, F.; Ergurrolla, U.; Vallat, M. F. *J. Adhes.* **2007**, *83*, 875−895.
(38) Airoudj, A.; Schrodj, G.; Vallat, M. F.; Roucoules, V. *Int. J. Adhes. Adhes.* **2001**, *31*, 498−506.
(39) Vautard, F.; Grappe, H.; Ozcan, S. *Appl. Surf. Sci.* **2013**, *268*, 61−72.
(40) Vance, A. L.; Willey, T. M.; Van Buuren, T.; Nelson, A. J.; Bostedt, C.; Fox, G. A.; Terminello, L. J. *Nano Lett.* **2003**, *3*, 81−84.
(41) Schultz, J.; Nardin, M. In *Modern Approaches to Wettability: Theory and Application*; Schrader, M. E.; Loeb, G., Eds.; Plenum Press: New York, 1992; pp 73−99.
(42) Greszczuk, L. B. In Theoretical studies of the mechanics of the fiber−matrix interface in composites. *Proceedings of the interfaces in composites, American Society for Testing and Materials Special Technical Publications (ASTM STP) 452*; American Society for Testing and Materials: West Conshohocken, PA, 1969; pp 42−58.
(43) Gao, S. L.; Mäder, E.; Zhandarov, S. F. *Carbon* **2004**, *42*, 515−29.
(44) Krzeminski, M.; Molinari, M.; Troyon, M.; Coqueret, X. *Macromolecules* **2010**, *43*, 3757−3763.
(45) Krzeminski, M.; Molinari, M.; Troyon, M.; Coqueret, X. *Macromolecules* **2010**, *43*, 8121−8127.
(46) Ponsaud, P. Improvement of the transverse mechanical properties of electron-beam cured composite materials. Ph.D. Thesis, Université des Sciences et Technologies de Lille, Lille, France, 2005.
(47) Schofield, W. C. E.; McGettrick, J.; Bradley, T. J.; Badyal, J. P. S.; Przyborski, S. *J. Am. Chem. Soc.* **2006**, *128*, 2280−2285.